Synthesis of short-wave infrared $Ge_{1-v}Sn_v$ semiconductors directly on Si(100) via ultralow temperature molecular routes for monolithic integration applications

Cite as: J. Vac. Sci. Technol. A 40, 063405 (2022); https://doi.org/10.1116/6.0002052 Submitted: 30 June 2022 • Accepted: 26 September 2022 • Published Online: 01 November 2022

🔟 Chi Xu, Ting Hu, Aixin Zhang, et al.







ARTICLES YOU MAY BE INTERESTED IN

Study of critical optical confinement factor for GeSn-based multiple quantum well lasers Applied Physics Letters 121, 171101 (2022); https://doi.org/10.1063/5.0107081

Impact of strain on Si and Sn incorporation in (Si)GeSn alloys by STEM analyses Journal of Applied Physics 132, 195306 (2022); https://doi.org/10.1063/5.0117300

Direct bandgap GeSn nanowires enabled with ultrahigh tension from harnessing intrinsic compressive strain

Applied Physics Letters 120, 202103 (2022); https://doi.org/10.1063/5.0087477







Synthesis of short-wave infrared $Ge_{1-v}Sn_v$ semiconductors directly on Si(100) via ultralow temperature molecular routes for monolithic integration applications

Cite as: J. Vac. Sci. Technol. A 40, 063405 (2022); doi: 10.1116/6.0002052 Submitted: 30 June 2022 · Accepted: 26 September 2022 · Published Online: 1 November 2022







Chi Xu, 🗓 Ting Hu, 2 Aixin Zhang, 2 Dhruve A. Ringwala, 2 José Menéndez, 1 📵 and John Kouvetakis 2.a)

AFFILIATIONS

- Department of Physics, Arizona State University, Tempe, Arizona 85287-1504
- School of Molecular Sciences, Arizona State University, Tempe, Arizona 85287-1604

ABSTRACT

We report the synthesis of $Ge_{1-y}Sn_y$ films containing 6%–13% Sn directly on Si(100) for monolithic integration applications, circumventing the use of conventional Ge-buffer layers. The films are produced in a gas source molecular epitaxy chamber at ultralow temperatures of 185-210 °C and a pressure of 10⁻⁵ Torr by the reactions of pure vapor Ge₄H₁₀ and SnD₄ or SnH₄ without carrier gases. Very small amounts of Si, incorporated via the Si₄H₁₀ precursor, can be used to improve the structural properties. All samples were characterized by XRD, RBS, IR-ellipsometry, AFM, and TEM, indicating the formation of monocrystalline single-phase films with relatively low defectivity and flat surfaces. A notable highlight is that the residual strains of the alloy layers are much lower compared to those grown on Ge buffers and can be further reduced by rapid thermal annealing without decomposition, indicating that growth on bare silicon should produce bulklike, high Sn content alloys that cannot be accessed using Ge buffers. N-type analogs of the above samples doped with phosphorus were also produced using P(SiH₃)₃ as the in situ dopant precursor. The results collectively illustrate the potential of our chemistry-based method to generate good quality $Ge_{1-\nu}Sn_{\nu}$ layers directly on large area Si wafers bypassing Ge buffers that typically lead to complications such as multiple hetero-interfaces and epitaxial breakdown at high Sn concentrations.

Published under an exclusive license by the AVS. https://doi.org/10.1116/6.0002052

I. INTRODUCTION

Alloys of Ge and Sn are the only group-IV semiconductor system with direct band gaps covering the near-, mid-, and long-wave infrared optical spectrum from 1.55 to $\sim 20 \,\mu m$ and potentially beyond. 1-5 This property enables unique applications in Si-based photonics, including lasing.^{6–9} A concerted effort has been devoted over the past two decades to develop CVD methods to grow Ge_{1–y}Sn_y alloy films. $^{10-16}$ Ge sources used range from GeH_4 or Ge_2H_6 hydrides, compatible with several industrial processes, to Ge₃H₈ or higher-order analogs used in custom reactors. The latter offer enhanced process capabilities and the ability to grow the alloys at lower temperatures, which extends the compositional range accessible with CVD. 17-19 In parallel with the effort to optimize the CVD route, molecular beam epitaxial (MBE) methods have also been refined to achieve high Sn

concentrations.²⁰ This approach was used in the early days of the field, 21,22 and it is attractive for its ability to grow the metastable alloy at temperatures sufficiently low to prevent Sn segregation.

In the recent work, we demonstrated that gas source molecular epitaxy (GSME), a hybrid of CVD and MBE, is a viable alternative for the growth of Ge_{1-v}Sn_v alloys on Si platforms that combines the advantages of the two major approaches.²³ Our GSME implementation is based on Ge₄H₁₀ as the Ge source and deuterated stannane SnD₄ (or SnH₄) as the Sn source. Growth proceeds at ultralow temperatures T < 210 °C and pressures $p \sim 10^{-5}$ Torr, which are conditions similar to those prevailing in molecular beam epitaxy (MBE). By contrast, UHV-CVD growths, which rely on Ge₂H₆ or Ge₃H₈ as Ge sources, 10,24,25 require temperatures of about 150 °C higher and are carried out in the presence of H2 flow at 0.2 Torr. The GSME films

a)Electronic mail: Jkouvetakis@asu.edu

possess excellent crystallinity, as evidenced by 004 x-ray rocking curves with low full width at half maximum (FWHM), and significant strain relaxation levels as-grown, which enable further relaxation by *ex situ* annealings. Alloys with Sn concentrations as high as 13% have been demonstrated, well beyond the indirect to direct gap crossover and reaching the onset of the middle wavelength infrared (MWIR) range.

The GSME growth of Ge_{1-y}Sn_y alloys described above was demonstrated on Ge-buffered Si wafers.²³ The intermediate Ge-buffer layers reduce the strain differential between the Ge_{1-y}Sn_y alloy and Si, allowing the growth of layers with high crystalline quality and relatively lower defectivities.²³ However, growth without buffer layers has distinct advantages, including significant cost savings. A device design devoid of buffer layers is more convenient to allow facile monolithic integration of photodetectors with readout integrated circuits (ROIC) near the 2-μm cut-off, an application that has received increased attention following the introduction of low-loss hollow-core photonic bandgap fibers.²⁶ Furthermore, devices grown directly on Si are amenable to effective back-illumination conditions to obtain enhanced photodetection at $1.55 \mu m$ and shorter wavelengths by eliminating the absorbing Ge-buffer layers. Methods relying on commercial reactors have made little progress to advance growth directly on Si, but UHV-CVD growths by our group that combine Ge₂H₆ or Ge₃H₈ with either SnD₄ or SnH₄ yield Ge_{1-y}Sn_y films directly on Si with concentrations as high as 36% Sn. 5,19 We note that a recent study reports SiGeSn growth directly on Si but with a very narrow range of 0.5%-2% Sn contents.²⁷ The success of our GSME approach described above for the growth on Ge-buffer layers suggests that the same method might also represent a viable alternative to UHV-CVD for growth directly on Si. The GSME method is more convenient, the reactor ambient is cleaner, mitigating unintentional doping, and the consumption of expensive and rare Ge is much more efficient. In this paper, we confirm this conjecture by reporting the growth of undoped and *n*-type $Ge_{1-y}Sn_y$ films with y = 6%-13% directly on 4 in. Si wafers using Ge₄H₁₀/SnD₄ or Ge₄H₁₀/SnH₄ precursors in a GSME chamber. SnD₄ has been historically preferred over SnH₄ due to its longer lifetime at room temperature. However, SnH₄ is more reactive and its use in place of SnD₄ became necessary to increase Sn incorporation beyond 12% while maintaining reasonable growth rates at the lowest temperatures. The synthesis results reveal noteworthy differences between $Ge_{1-\nu}Sn_{\nu}$ -on-Si over $Ge_{1-\nu}Sn_{\nu}$ -Ge-Si analogs. These include better strain relaxation for direct growth on Si, and smoother surfaces devoid of cross-hatch patterns. The ultralow temperature GSME Ge₄H₁₀ route described here (involving benign hydride chemistry with noncorrosive byproducts) may provide a pathway for the synthesis of Ge_{1-y}Sn_y layers directly on thermally and chemically sensitive Si ROICs. We also find that the crystallinity of the resultant layers directly on Si is better relative to analogous samples grown by UHV-CVD, and the film thicknesses can be extended as needed to achieve the device specifications. Such layers could be used to fabricate monolithically integrated detectors operating in the short-wave infrared (SWIR) or MWIR spectral region.

II. EXPERIMENTAL DETAILS

A. General considerations

The challenge of growing directly on Si substrates using GSME is the much lower temperature regime, which might affect

the generation of the misfit defects that accommodate the enormous lattice mismatch between $\rm Ge_{1-y}Sn_y$ and Si. To mitigate possible deleterious effects, we carried out our initial experiments by introducing a small Si fraction (~1%) using the tetrasilane $\rm Si_4H_{10}$ precursor. Such levels of Si incorporation have a very small effect on the structural and electronic properties of the alloy, but the availability of Si at the GeSn/Si interface may promote a smoother transition from one material to the other resulting to better crystallinity epilayers. After successfully demonstrating growth following this approach, we also grew samples completely devoid of Si.

The GSME reactor in which the growth of the Si-doped Ge_{1-v}Sn_v alloys was conducted is a single wafer UHV system with a base pressure of 10⁻¹⁰ Torr. It provides a clean background for the fabrication of epitaxial crystals with pure interfaces at conditions akin to MBE.²² Working pressures of 10⁻⁵ Torr and temperatures between 185 and 300 °C are employed for growth in this system. Tetragermane (Ge₄H₁₀), tetrasilane Si₄H₁₀, and stannanes SnD₄ or SnH₄ were specifically selected as sources of Ge, Si, and Sn, respectively. P(SiH₃)₃ was used to produce n-type samples doped with P and Si atoms. These molecules are heavy and adsorb readily on the growth surface under the ultralow pressures employed, binding with multiple points of contact and reacting readily at T > 180 °C by releasing hydrogen. In the case of Ge₄H₁₀, the Ge-H bonds are weaker compared to Ge₂H₆ and Ge₃H₈ analogs, and thus easier to activate at ultralow temperatures, making the compound an ideal Ge source for low pressure/temperature CVD. The high mass of Ge₄H₁₀ also reduces surface mobility, making it possible to pin the molecular cores intact on the growth front where they combine and effectively react with Sn hydrides that exhibit compatible reactivity. In general, lower order Ge and Si hydrides do not react under the ultralow pressures/temperatures conditions of our GSME technique to produce Si-Ge-Sn films, presumably due to reduced sticking coefficients. Furthermore, low mass dopants such as PH₃, AsH₃, and B₂H₆ are also unreactive, in contrast to heavier P(SiH₃)₃. This suggests that the molar mass is an important parameter to consider when designing these GSME experiments.

 Ge_4H_{10} is synthesized in-house by thermolysis of commercial Ge_2H_6 , and it is isolated as a colorless liquid exhibiting a vapor pressure of 1 Torr at room temperature. Si_4H_{10} is a colorless liquid with a vapor pressure of 20 Torr, which makes it perfectly suitable for CVD applications. 28,29 Si_4H_{10} is preferred in this study over the standard SiH_4 and Si_2H_6 sources due to its higher reactivity, which enables the formation of crystalline films at $T \sim 200~^{\circ}\text{C}$ at practical growth rates. The Sn hydrides SnD_4 and SnH_4 are synthesized in-house as needed and stored under liquid nitrogen to avoid decomposition. $P(SiH_3)_3$ is synthesized as a colorless volatile liquid with $\sim 20~\text{Torr}$ vapor pressure. Reactions of the compound incorporate the entire PSi_3 molecular core—presumably intact—into the film at ultralow temperatures, delivering high n-carrier concentrations with near full activation. 30

Films in this study were grown directly upon Si p-type 4 in.-wafers with a resistivity of $10-20\,\Omega$ cm. The substrates were first RCA cleaned and then dipped in a 5% HF/methanol bath to passivate their surface with hydrogen. They were then flashed at 800 °C under UHV to remove any remaining oxide impurities and generate a pure surface. A vessel containing pure Ge_4H_{10} supply and another one containing a mixture of Si_4H_{10} /SnD₄ were attached to different



TABLE I. Summary of growth parameters and materials properties of Ge_{1-v}Sn_v films (y = 0.06-0.13) grown directly on Si(100). Three separate sets of samples are described including intrinsic alloys doped with 1%-2% Si, intrinsic alloys without Si, and n-type analogs, doped with P. Samples A-J and L-O were grown using SnD₄. Sample K was grown using SnH4. In all cases, Sn incorporation increases with decreasing temperature. The residual in-plane strains diminish with increasing Sn content in each category in the table. The temperatures listed and those mentioned throughout this paper correspond to the heater and not the substrate surface, which is typically 10-20 °C lower.

Sample code	Sn%	Si%	Growth T (°C)	Thickness (nm)	Strain (%)	Doping (cm ⁻³)
GeSn(Si)						_
A	6.5	1	215	760	-0.38	
В	7	1	210	430	-0.27	
C	8	1	205	540	-0.27	
D	8.5	1	200	350	-0.30	
E	11	2	190	140	-0.17	
F	12	1	190	150	-0.12	
GeSn						
G	6	0	215	390	-0.39%	
H	9.4	0	205	100	-0.21%	
I	9.7	0	200	185	-0.20%	
J	11	0	195	75	-0.16%	
K	13	0	190	80	-0.09%	
n GeSn(Si)						
L	7.2	1	210	265	-0.42	2×10^{19}
M	7.8	2	203	410	-0.38	3×10^{19}
N	10.5	1	195	300	-0.36	3×10^{19}
О	10	2	200	200	-0.28	2.3×10^{19}

gas inlets of the reactor, allowing independent control of the gaseous flux using leak valves. In any given run, pure Ge₄H₁₀ was first released into the chamber at a pressure of $2-3 \times 10^{-6}$ Torr followed by the Si₄H₁₀ /stannane mixture, raising the total combined pressure in the range of $2-3 \times 10^{-5}$ Torr. The gas flow was occasionally adjusted to maintain the pressure stable inside the chamber throughout the course of the experiment. We note that premixing desired amounts of Si₄H₁₀ and stannane into a single gas supply facilitated control of the Si stoichiometry in the reaction medium and ensured the uniformity of the atomic distribution. The amount of stannane utilized per run varied from 15-30 L × Torr depending on the amount of time needed to generate the desired film thickness. Both intrinsic layers and n-type analogs were grown under these conditions. For the growth of the latter films, a suitable amount of P(SiH₃)₃ was combined with Si₄H₁₀ and stannane in the same container and delivered together to the growth surface. Intrinsic layers without Si were grown using the same protocols as those doped with Si.

B. Growth of intrinsic Ge_{1-y}Sn_y (Si)

The experiments in this case lasted 2-3 h and produced thick layers with visually smooth, mirrorlike surfaces and no sign of Sn segregation. Table I lists the growth conditions and materials properties of representative alloys doped with Si (first six rows), intrinsic samples without Si (middle rows), and n-type analogs doped with P (bottom rows). In all cases, the growth parameters, including reactants ratio, growth time, and reaction temperature and pressure, were iteratively fine-tuned and optimized to produce the desired compositions and thickness in the fabricated samples. Ellipsometry and Rutherford backscattering (RBS) were routinely used to measure the thickness and elemental content, respectively. The results showed that 6%-12% Sn alloys were obtained using SnD₄ by systematically lowering the growth temperature from 215 ° C to 190 °C, respectively. It was observed that keeping the temperature constant and increasing the SnD₄ partial pressure did not affect the Sn concentration. However, a slight increase in the growth rate was obtained. The Si concentration in the Si-doped samples was kept constant for all samples at 1%-2% by slightly adjusting the amount of Si₄H₁₀ used in the reaction medium in a given run.

The need to lower the growth temperature to achieve higher Sn content resulted in lower growth rates and layer thicknesses. For example, the 6% films shown in the first line of Table I were produced with a growth rate of ~3-4 nm per min, generating final thicknesses of 750 nm and beyond, as required for future fabrication of 2-μm photodetectors with 6%Sn active layers. For the 10%– 12% Sn samples, the growth rate dropped significantly with temperature to ~1-2 nm/min. In this case, extending the deposition time was necessary to produce thicknesses between 80 and 300 nm that allow meaningful characterization of the resultant materials, as discussed below. The data in general revealed that viable samples can be synthesized using this approach with compositions in the direct gap regime and with suitable morphology and structure for applications as passive layers on Si. Pushing the Sn concentration beyond 12%, however, becomes impractical using SnD₄ due to further reduction in growth rates. In this case, we utilized the more reactive SnH₄ to extend the Sn content to 13% (sample K), covering the SWIR range from 2 to $3 \mu m$.

High resolution XRD (HRXRD) was used to determine crystallinity, strain states, and Sn compositions. Figure 1 shows representative spectra for a film grown at ~ 195 °C. The blue trace

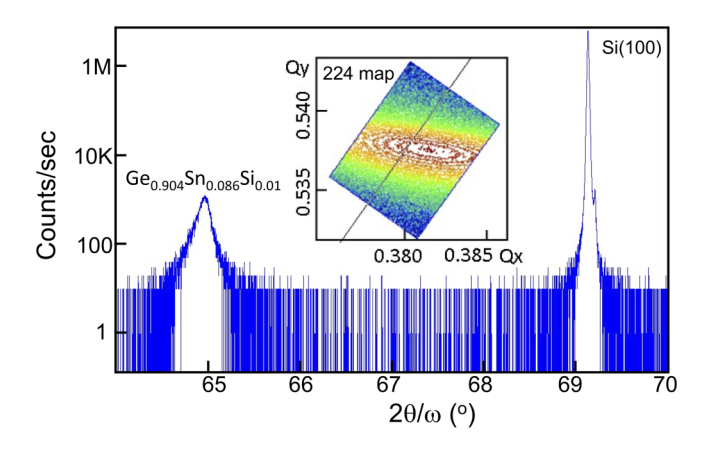


FIG. 1. XRD plots showing 004 peak (blue line) and 224 RSM (the inset) for the 8.6% Sn sample "as-grown" on Si. The relaxation line passes above the epilayer peak, indicating residual compressive strain of 0.27%. Q_x and Q_y are measured in reciprocal lattice units (rlu). $Q_y(001) = (2\lambda/c)$, where $\lambda = 1.5405$ Å and c is the vertical lattice parameter. $Q_x(110) = \lambda \sqrt{2/a}$, where a is the horizontal parameter.

corresponds to the on-axis scan showing the sharp 004 reflection of the diamond structure. The corresponding reciprocal space map (RSM), shown in the inset, illustrates a well-defined single peak in the vicinity of the 224 reflection. The relaxation line passes slightly above the peak maximum, indicating the presence of a slight compressive strain. This was measured to be 0.27%, which is about the average of all films produced in this study as shown in Table I. The in-plane and vertical lattice constants of the distorted unit cell in this sample were measured to be a = 5.711 Å and c = 5.738 Å,

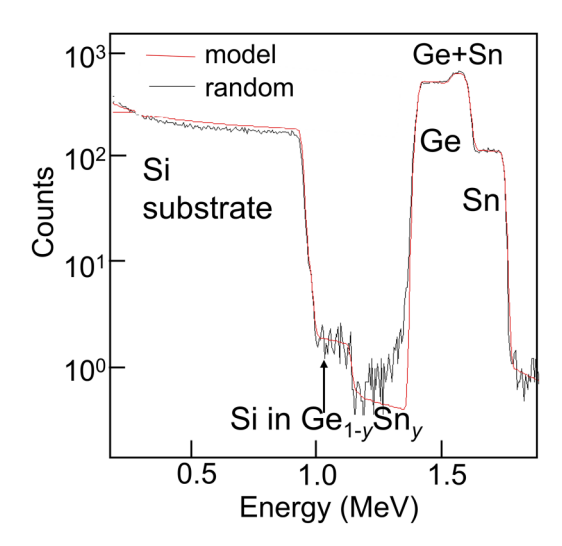


FIG. 2. RBS random spectrum (black line) and the thickness/composition model fit (red line) of a 360 nm thick layer with \sim 8.6% Sn and 1% Si. The film Si signal is visible slightly above the background, as marked with arrow.

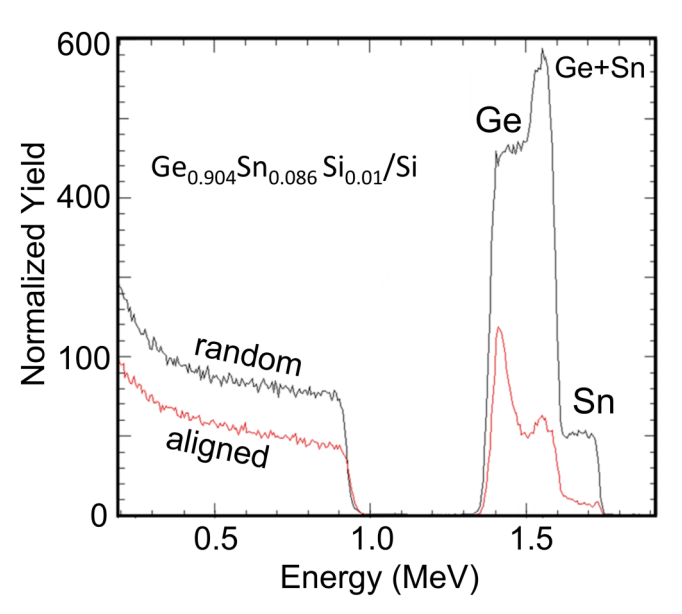


FIG. 3. RBS random (black) and channeled (red) spectra of $Ge_{0.904}Sn_{0.086}Si_{0.01}$ on Si. The high degree of channeling indicates good crystallinity, epitaxial alignment, and Sn substitutionality.

respectively, and used to calculate a relaxed cubic constant $a_0 = 5.727$ Å. In conjunction with Vegard's law, this yields a composition of 8.6% Sn using a Si concentration of 1%. The Si fraction was directly measured by RBS, which also provided the absolute bulk Sn and Ge contents as well as the layer thickness.

Figure 2 is a logarithmic plot of an RBS spectrum measured at 2 MeV, illustrating the presence of distinct and strong Sn and Ge plateaus from the film. The corresponding Si contribution is shown as a low-intensity plateau emerging above the baseline at the onset of the Si wafer background. The flat profile of the plateaus indicates that the atomic species are distributed homogeneously throughout the entire layer thickness. The model fit of the spectrum, shown by

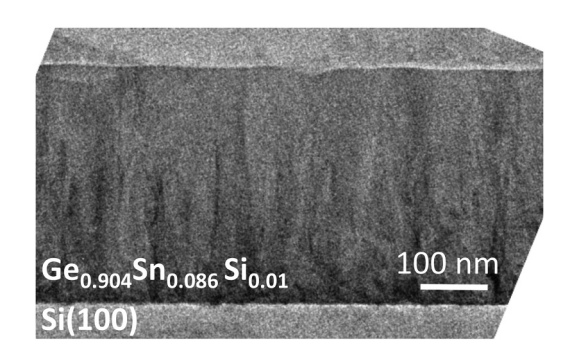


FIG. 4. XTEM image for \sim 8.6% Sn, 360 nm thick layer doped with 1%Si. The image shows the full epilayer, illustrating a monocrystalline structure and flat surfaces of the film. No Sn precipitation and phase segregations are visible.

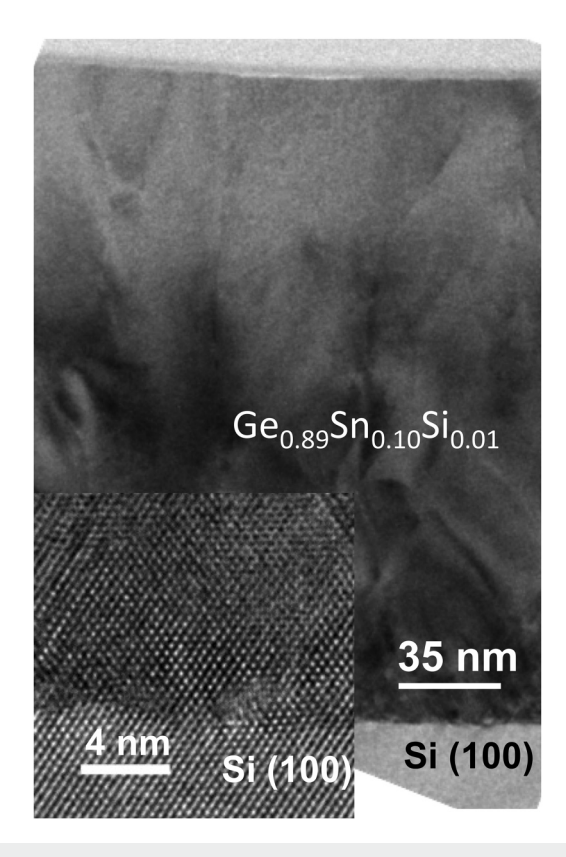


FIG. 5. Main panel shows the XTEM image of the 260 nm $Ge_{0.89}Sn_{0.10}Si_{0.01}$ film on Si. The film is defected mostly in the lower part near the interface. The inset shows the high resolution image of the Si interface, indicating that the layer is epitaxial.

the red line, yielded a composition of $Ge_{0.904}Sn_{0.086}Si_{0.01}$ and a thicknesses of 360 nm. Modeling of the data using both the program RUMP and SMRA indicated that the error of the Si contents is 0.5%.

Figure 3 shows linear plots of the 2 MeV random and aligned RBS spectra of the same sample. The high degree of channeling is manifested by the significant reduction of the backscattering signal intensity of the aligned spectrum relative to the random one, indicating that the layer is monocrystalline and epitaxial. The uniform channeling is also consistent with the Sn atoms occupying substitutional sites in the Ge lattice, producing a single-phase alloy. The substitutionality of Sn is further corroborated by the identical RBS and XRD Sn concentrations of ~8.6%.

Cross-sectional transmission electron microscopy (XTEM) was used to investigate the microstructure. A high resolution image of the 8.6% Sn sample is presented in Fig. 4. The image reveals a uniform epilayer, exhibiting a high density of defects near the interface region, while the upper part is relatively less defected and terminates in a flat top surface. The diffraction contrast appears homogeneous throughout with no discernible secondary phases due to Sn precipitation, indicating that the material is the single-phase alloy, in agreement with the XRD results.

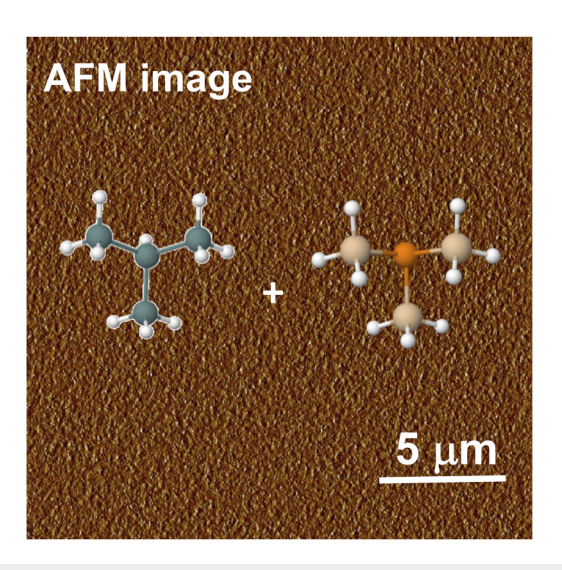


FIG. 6. $20 \times 20 \,\mu\text{m}$ AFM image for an *n*-type GeSiSn sample with 7.2% Sn, 1% Si, and 370 nm thickness. The RMS roughness is 1.7 nm. Molecular structures of Ge₄H₁₀ (branched conformation) and P(SiH₃)₃ coreactants are shown.

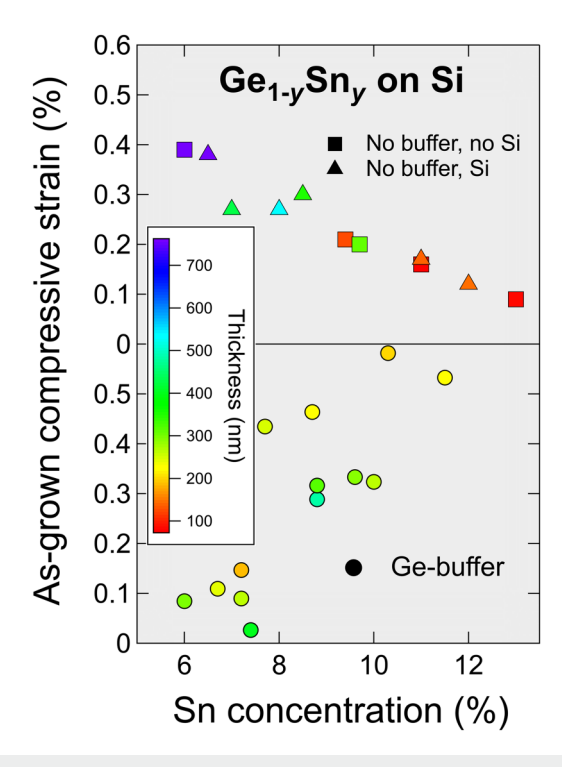


FIG. 7. As-grown compressive strain in $Ge_{1-y}Sn_y$ samples grown on Si. Circles are data from Ref. 23, which describes samples grown on Ge buffers. Squares and triangles correspond to samples grown for this work directly on Si without buffer layers. Squares correspond to samples that contain no Si and triangles to samples with contain minor amounts of Si, as shown in Table I.

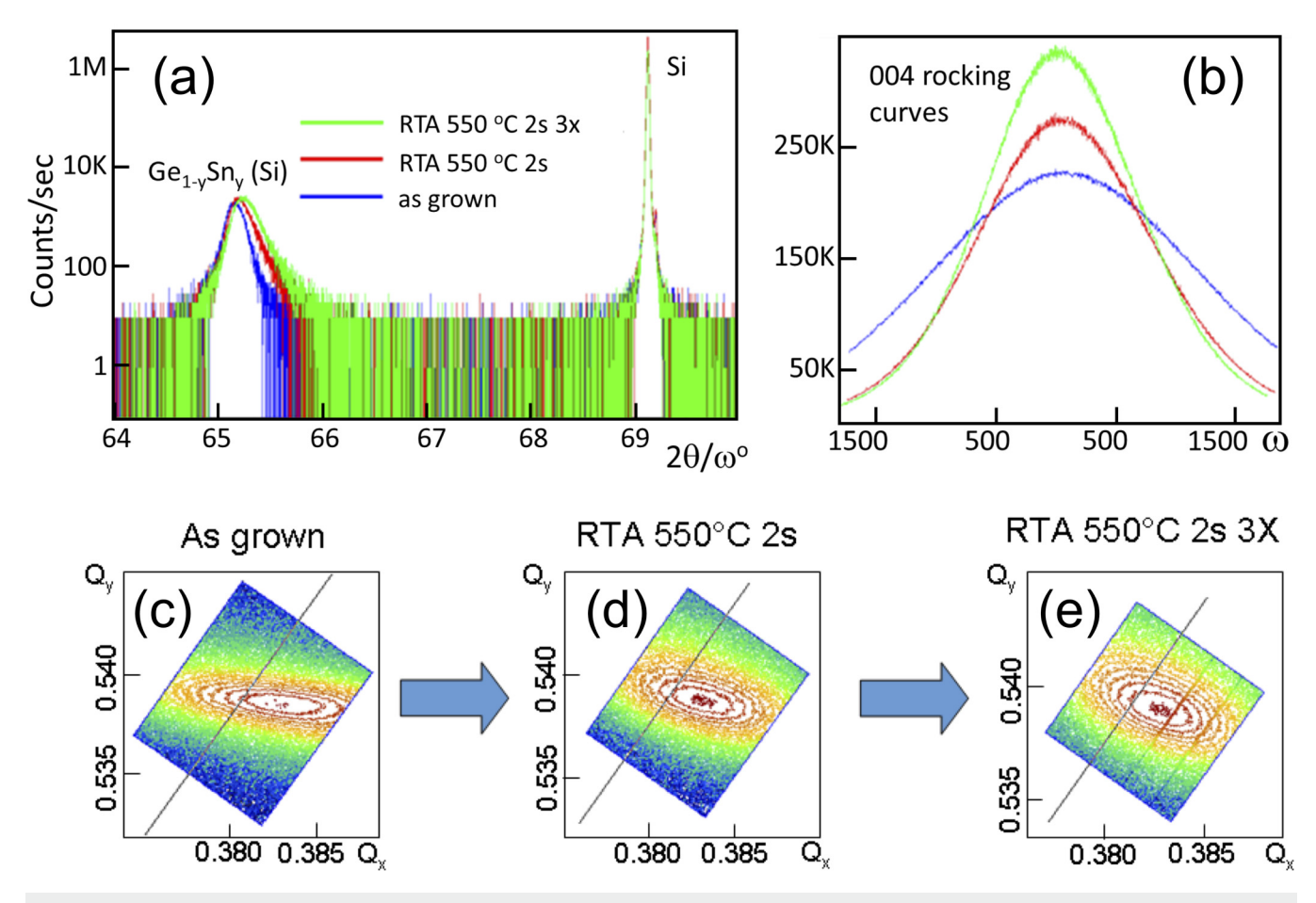


FIG. 8. (a) XRD θ-2θ scans for a 760 nm thick film with 6.5% Sn and 1% Si, showing the 004 peaks of the as-grown sample (blue line), annealed at 550 °C 2 s (red), and annealed at 550 °C, 2 s, three times (green). (b) Rocking curves of the same sample under such treatments; (c)–(e) show corresponding XRD 224 RSM peaks (and relaxation lines) revealing that compressive strain decreases and the shape of peak is more rounded and compact due to improvements in mosaic spread.

TEM images of a different 10% Sn sample with 260 nm thickness are shown in Fig. 5. The bulk layer in this case is also monocrystalline and hetero-epitaxial as shown by a high resolution image (inset) of the interface with Si. The mismatch-induced defects are concentrated near the bottom region, while the upper part exhibits a significantly improved microstructure as evidenced by the presence of fewer dislocations that penetrate toward the surface. The latter is flat, which is consistent with AFM measurements with RMS roughness in the range of $\sim 2{\text -}3$ nm. No cross-hatch patterns are observed in these materials grown on Si, in contrast to films grown on Ge buffers. The above structural and morphological results collectively show that the layers grown directly on Si exhibit good crystallinity and mostly relaxed strain states.

C. Growth of n-type samples

With device development in mind, we also pursued proof of concept growth of *n*-type layers analogous to the intrinsic

counterparts containing Si. We envision the development of homostructure pin diodes in which the bottom contact comprises a thick n-type $Ge_{1-y}Sn_y$ (Si) film grown directly upon Si followed by an intrinsic counterpart with a slightly higher Sn content in the mid-IR. A series of such n-doped $Ge_{1-y}Sn_y$ samples containing 1%-2% Si were grown, and representative examples are listed in Table I. The emphasis was placed on developing films with large thicknesses above 200 nm to facilitate the formation of electrical contacts, and high Sn contents in the direct bandgap regime to be used not only as contacts but also as buffer layers for direct integration of light emitting devices with Si at CMOS compatible temperatures. The experiments utilized 4-in. wafers as substrates and Ge_4H_{10} and SnD_4 as the Ge and Sn sources, respectively.

 $P(SiH_3)_3$ was used as the source of both P and Si. The latter was augmented by adding small amounts of Si_4H_{10} in the reaction mixtures producing samples with \sim 7–11% Sn, \sim 1–2% Si, and 2–3 \times 10¹⁹ cm⁻³ active carrier concentrations. The thickness of the films ranged from \sim 200 to 400 nm which is sufficient for electrical

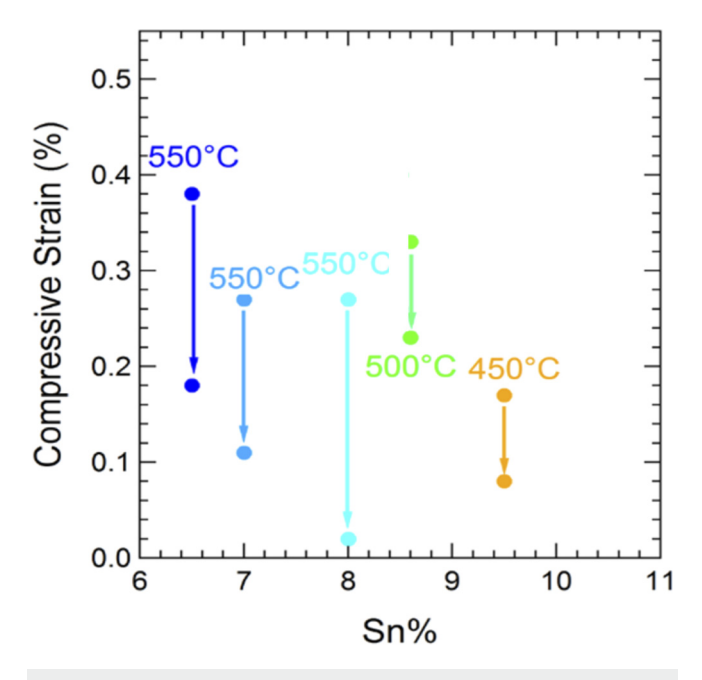


FIG. 9. Plot of residual strain before and after annealing vs composition. A sizable decrease in compressive strain is observed for all RTA treated samples.

contact purposes. The active carrier levels were modeled by IR-ellipsometry and are listed in Table I. RBS, XTEM, and XRD analyses were routinely used to characterize the samples, and the results indicated comparable crystallinity and strain states to the intrinsic samples. The residual compressive strains gradually decreased with the increasing Sn content due to the ever increasing mismatch with the Si substrate. One noteworthy observation is that the roughness of the doped layers was lower than that of the intrinsic analogs. Figure 6 shows an AFM image of a 7.2% Sn sample exhibiting a flat surface with 1.7 RMS roughness. The latter morphology makes the materials perfectly suitable for subsequent integration of devices, mitigating the lattice mismatch between the substrate and higher Sn epilayers. Such n-layers grown directly on Si(100) substrates would be the best choice to circumvent the need for Ge-buffer layers entirely. This strategy also simplifies the system by eliminating the complication of multiple hetero-interfaces that in the case of GeSn devices contain mismatched induced defects that increase nonradiative recombination.³

D. Growth of samples without silicon

Following the successful growth of Si-doped samples, we also produced $Ge_{1-y}Sn_y$ alloys without Si doping. Representative examples with high Sn content are listed in middle rows of Table I. In general, we observed that the growth rates and residual strains are similar to those for samples containing silicon. One intriguing difference and potential benefit of incorporating Si at the small 1%-2% levels used is that an enhanced crystallinity is evidenced by lower widths of the 004 rocking curves. Taken together, the results

demonstrated that the reproducibility and repeatability of the synthesis were improved when ${\rm Si_4H_{10}}$ was added to the reaction medium in our experiments.

E. Strain relaxation

The as-grown strain values for the intrinsic samples in Table I are displayed graphically in Fig. 7, which also shows for comparison similar data for alloys grown on Ge-buffered Si from Ref. 23. The samples grown directly on Si display residual compressive strains that gradually decrease from 0.38% for the 6% Sn sample to 0.12% for the 12% Sn sample, down from a lattice mismatch of 4.8% and 5.7%, respectively, between the alloy films and the Si substrate. The amount of strain relaxation is largely independent of thickness, as shown color-coded in Fig. 7.

We also note that the increased strain relaxation at high Sn concentration occurs even though these samples are grown at lower temperatures. The behavior of the samples grown on Ge buffers is markedly different. Here, the lattice mismatch between the film and buffer layer runs from 0.9% to 1.7%, and the residual strain increases for the high-Sn samples that are grown at lower temperatures. This phenomenology is consistent with existing theories of strain relaxation that have been applied to the GeSn and SiGe systems. 32-34 The mechanism behind the observed strain relaxation in the samples grown directly on Si is more complex. The independence of thickness and growth temperature suggests that the strain relaxation is a purely interfacial effect that will require detailed microscopic studies to unravel. We find that the progressive mismatch with Si also induces a broadening of the 004 rocking curves, which show FWHM in the vicinity of 0.5°-0.7° in our experiments. These values are larger compared to the samples grown on Ge buffers, indicating that the mosaicity is higher.

To further reduce the remaining strains and improve the mosaic spread, selected 6%–10% Sn samples were subjected to rapid thermal annealing (RTA) treatments. The annealing time was chosen to be 2 s cycles to avoid degradation of the materials. The 6% Sn sample was annealed at a maximum temperature of 550 °C for several cycles, reducing its strain from 0.38% down to 0.18%. Panel (a) in Fig. 8 shows 004 XRD plots before annealing (as-grown) and after annealing for 2 s one time and 2 s three times. The peaks shift slightly toward higher diffraction angles (lower *c*-spacing), which is consistent with strain relaxation. The corresponding 224 reciprocal space maps are shown in panels (c)–(e), illustrating that the peaks become more symmetrical upon annealing, presumably due to improvements in the mosaic spread. The latter is corroborated by a concomitant narrowing of the FWHM of the 004 rocking curves from 0.6° to 0.42° as shown by the plots in panel (b).

Figure 9 summarizes the changes in strain for alloys with up to 9.5% Sn subjected to RTA treatments. The maximum annealing temperature allowed for these samples decreases with increasing the Sn content to prevent decomposition. We notice that the 0.27% strain for the 8% Sn sample is virtually removed at 550 °C, while the strains of the 8.5%Sn and 10%Sn samples are reduced down to 0.23% and 0.06% upon annealing at \sim 500 and 450 °C, respectively. In all cases, the thermal treatments induce a significant relaxation without degrading surface morphology and phase purity. With



regard to the latter, we note that the RBS Sn content was virtually identical to that measured by XRD of the annealed samples, indicating that no Sn segregation occurred under the RTA conditions employed in our experiments. Refinement of the heat treatments is ongoing, and the results show that RTA can be routinely and effectively used for processing materials grown directly on Si.

III. SUMMARY

We demonstrated the development of intrinsic and n-type $Ge_{1-y}Sn_y$ layers directly on Si with Sn contents up to \sim 12% by reactions of Ge_4H_{10} and SnD_4 at ultralow temperatures of 190–210 °C. Sn contents beyond 12% required the use of the more reactive SnH_4 precursor in place of SnD_4 . Materials doped with 1%-2% Si show an improvement in their structural properties, promoting the formation of flat and smooth surfaces devoid of defects and precipitates. The resultant samples exhibit large thickness (up to 750 nm), good crystallinity, and near full strain relaxation due to the large lattice misfit with Si, making them suitable for applications as platforms for the growth of devices directly on Si, circumventing the use of the conventional Ge-buffer layers. This may be particularly advantageous for the subsequent growth of $Ge_{1-y}Sn_y$ with y > 0.20 with improved structural and optical properties.

ACKNOWLEDGMENT

This work was supported, in part, by the National Science Foundation under Grant No. DMR-2119583.

AUTHOR DECLARATIONS

Conflict of Interest

The authors have no conflicts to disclose.

Author Contributions

Chi Xu: Investigation (equal). Ting Hu: Investigation (equal). Aixin Zhang: Investigation (equal). Dhruve A. Ringwala: Investigation (equal). José Menéndez Investigation (equal). John Kouvetakis: Project administration (equal); Supervision (equal); Writing – review & editing (equal).

DATA AVAILABILITY

The data that support the findings of this study are available within the article. Further questions about supporting data should be send to the corresponding author.

REFERENCES

¹S. Wirths, D. Buca, and S. Mantl, Prog. Cryst. Growth Charact. Mater. 62, 1 (2016)

- ²J. Mathews, R. T. Beeler, J. Tolle, C. Xu, R. Roucka, J. Kouvetakis, and J. Menéndez, Appl. Phys. Lett. 97, 221912 (2010).
- ³J. D. Gallagher, C. L. Senaratne, J. Kouvetakis, and J. Menéndez, Appl. Phys. Lett. **105**, 142102 (2014).
- ⁴S. Gupta, B. Magyari-Köpe, Y. Nishi, and K. C. Saraswat, J. Appl. Phys. 113, 073707 (2013).
- ⁵M. A. Mircovich, C. Xu, D. A. Ringwala, C. D. Poweleit, J. Menéndez, and J. Kouvetakis, ACS Appl. Electron. Mater. 3, 3451 (2021).
- ⁶S. Wirths et al., Nat. Photonics 9, 88 (2015).
- ⁷J. Margetis et al., ACS Photonics 5, 827 (2018).
- ⁸W. Dou et al., Opt. Lett. **43**, 4558 (2018).
- ⁹Y. Zhou et al., Optica 7, 924 (2020).
- ¹⁰M. Bauer, J. Taraci, J. Tolle, A. V. G. Chizmeshya, S. Zollner, D. J. Smith, J. Menendez, C. Hu, and J. Kouvetakis, Appl. Phys. Lett. 81, 2992 (2002).
- ¹¹B. Vincent et al., Appl. Phys. Lett. **99**, 152103 (2011).
- ¹²G. Grzybowski, L. Jiang, R. T. Beeler, T. Watkins, A. V. G. Chizmeshya, C. Xu, J. Menéndez, and J. Kouvetakis, Chem. Mater. 24, 1619 (2012).
- ¹³J. Margetis et al., ECS Trans. 64, 711 (2014).
- ¹⁴N. von den Driesch et al., Chem. Mater. 27, 4693 (2015).
- 15S. Assali, J. Nicolas, and O. Moutanabbir, J. Appl. Phys. 125, 025304 (2019).
- ¹⁶B. Claflin, G. J. Grzybowski, M. E. Ware, S. Zollner, and A. M. Kiefer, Front. Mater. 7, 44 (2020).
- ¹⁷J. D. Gallagher, C. L. Senaratne, C. Xu, P. Sims, T. Aoki, D. J. Smith, J. Menéndez, and J. Kouvetakis, J. Appl. Phys. 117, 245704 (2015).
- ¹⁸C. L. Senaratne, P. M. Wallace, J. D. Gallagher, P. E. Sims, J. Kouvetakis, and J. Menéndez, J. Appl. Phys. **120**, 025701 (2016).
- ¹⁹C. Xu, P. M. Wallace, D. A. Ringwala, S. L. Y. Chang, C. D. Poweleit, J. Kouvetakis, and J. Menéndez, Appl. Phys. Lett. 114, 212104 (2019).
- ²⁰S. Zaima, O. Nakatsuka, N. Taoka, M. Kurosawa, W. Takeuchi, and M. Sakashita, Sci. Technol. Adv. Mater. 16, 043502 (2015).
- ²¹P. R. Pukite, A. Harwit, and S. S. Iyer, Appl. Phys. Lett. **54**, 2142 (1989).
- ²²M. T. Asom, E. A. Fitzgerald, A. R. Kortan, B. Spear, and L. C. Kimerling, Appl. Phys. Lett. 55, 578 (1989).
- ²³C. Xu, T. Hu, D. A. Ringwala, J. Menéndez, and J. Kouvetakis, J. Vac. Sci. Technol. A **39**, 063411 (2021).
- ²⁴F. Gencarelli, B. Vincent, L. Souriau, O. Richard, W. Vandervorst, R. Loo, M. Caymax, and M. Heyns, Thin Solid Films 520, 3211 (2012).
- ²⁵G. Grzybowski, R. T. Beeler, L. Jiang, D. J. Smith, J. Kouvetakis, and J. Menéndez, Appl. Phys. Lett. 101, 072105 (2012).
- ²⁶X. Li, L. Peng, Z. Liu, Z. Zhou, J. Zheng, C. Xue, Y. Zuo, B. Chen, and B. Cheng, Photonics Res. 9, 494 (2021).
- ²⁷A. Mosleh et al., J. Electron. Mater. **45**, 2051 (2016).
- ²⁸R. T. Beeler, C. Xu, D. J. Smith, G. Grzybowski, J. Menendez, and J. Kouvetakis, Appl. Phys. Lett. **101**, 221111 (2012).
- ²⁹R. Hazbun, J. Hart, R. Hickey, A. Ghosh, N. Fernando, S. Zollner, T. N. Adam, and J. Kolodzey, J. Cryst. Growth 444, 21 (2016).
- ³⁰A. V. G. Chizmeshya, C. Ritter, J. Tolle, C. Cook, J. Menendez, and J. Kouvetakis, Chem. Mater. 18, 6266 (2006).
- ³¹J. D. Gallagher, C. L. Senaratne, C. Xu, P. Sims, T. Aoki, D. J. Smith, J. Menendez, and J. Kouvetakis, J. Appl. Phys. 117, 245704 (2015).
- ³²D. C. Houghton, J. Appl. Phys. **70**, 2136 (1991).
- 33 J. Menéndez, J. Appl. Phys. 105, 063519 (2009).
- ³⁴C. L. Senaratne, J. D. Gallagher, L. Jiang, T. Aoki, D. J. Smith, J. Menendez, and J. Kouvetakis, J. Appl. Phys. 116, 133509 (2014).